Digital Object Identifier (DOI): 10.1109/APEC.2018.8341232

Applied Power Electronics Conference and Exposition (APEC), 2018 IEEE

Smart Transformer Universal Operation

Youngjong Ko
Andrii Chub
Levy Costa
Markus Andresen
Marco Liserre

Suggested Citation

Y. Ko, A. Chub, L. Costa, M. Andresen and M. Liserre, "Smart transformer universal operation," *2018 IEEE Applied Power Electronics Conference and Exposition (APEC)*, San Antonio, TX, 2018, pp. 1609-1616.

Smart Transformer Universal Operation

Youngjong Ko, Andrii Chub, Levy Costa, Markus Andresen and Marco Liserre
Chair of Power Electronics, University of Kiel, Kiel, Germany
Email: {yoko, anc, lfc, ma, ml}@tf.uni-kiel.de

***Abstract*—The Smart Transformer (ST) has been proposed for increasing the hosting capacity of renewable energy sources in the power system with advanced control and communication capability. Its capability to connect- and disconnect itself from the main grid and to provide power from the Low Voltage (LV) grid to the Medium Voltage (MV) grid in the grid forming mode are an opportunity to realize an islanded operation mode. This operation mode requires a suitable controller design, which is forming the MV grid and the LV grid at the same time. This work proposes a modular ST architecture consisting of a three phase Cascaded H-Bridge (CHB) converter connected to Quadruple Active Bridge (QAB) converters. The design of the converter and its magnetic components is examined as well as the controller design for the QAB for the capability to address different operation modes. Grid forming operation on the both AC grid sides and the resulting constraints by means of active power availability are examined as well as opportunities to influence the power consumption of the grids. An experimental setup is presented and selected operation modes are demonstrated.**

***Index Terms*—Smart Transformer, Cascaded H-Bridge, Quadruple Active Bridge, Hardware Design, Grid forming mode**

I. Introduction

The increasing number of distributed generators, energy storage systems and new loads like electric vehicle charging stations connected to the electrical distribution grid challenges the hosting capacity for renewable energy sources. Along with the declining relevance of centralized power plants in some countries, the necessity to investigate a novel intelligent node in the electric grid is arising [1], [2]. The Smart Transformer (ST) as the interface between the Medium Voltage (MV) grid and the Low-Voltage (LV) grid is a promising solution for managing the power flow with high flexibility, providing services to the grid and enabling DC grid connectivity [3], [4].

The potential connection of the ST to four different grid voltages (MVAC, MVDC, LVAC and LVDC), which is shown in Fig. 1, poses a challenge for the control of the system. Traditional transformers only provided galvanic isolation and voltage adaptation, whereas converters of renewable energy sources commonly operate in the grid feeding mode. In the context of microgrids, the grid forming mode and grid supporting mode has gained attention [5]–[8]. The grid forming mode generates the grid with the voltage and frequency command, whereas the grid supporting mode makes the power converter a controllable current source or voltage source. The operation modes described are also expected to apply for the ST. As a resulting challenge, grid forming operation can be required in the LV side, the MV side or even on both sides at the same time. However, the challenge is to control the power flow in the system and to supply all loads while minimizing the active power exchange of the storage elements at the same time.

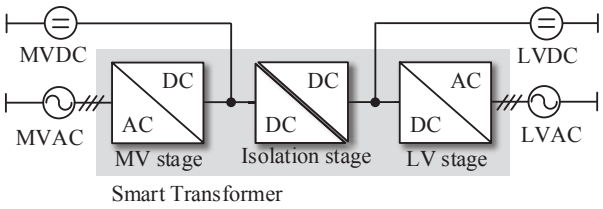

Fig. 1: Potential connection of the ST.

For all operation modes, the power needs to be balanced and therefore absorbed and injected in the connected feeders. Particularly grid feeding mode on both ac terminals is a challenge, which requires to absorb the required power from the DC-links, which can either be DC grids or energy storage systems. The connecting of energy storage systems to the DC ports of the system may be a potential solution to enable this operation mode for a certain time period. However, because of potentially limited generation in the DC grids or limited line capacity, it may be mandatory to control the generation and the load in the connected grids. An opportunity to achieve this is to control the voltage and the frequency in the AC grids and the voltage in the DC grid [9]–[11]. The voltage can be controlled and depending on the sensitivity, the load can be increased or decreased. The variation of the frequency in the AC grid is acting on the droop control of the distributed generators, potentially increasing or decreasing the generation.

This work describes a semi-modular ST design with a focus on the design of the magnetic components. In addition, different control modes of the ST in different grid conditions are described, highlighting challenges and potential drawbacks. A MV scale ST prototype consisting of a Quadruple Active Bridge (QAB) connected to a Cascaded H-Bridge Converter (CHB) in the MV stage is used to demonstrate the grid forming mode for a demonstration of the proposed concept.

First, this work describes the ST architecture with the hardware design of the stages in section II and the potential different control variables for affecting the power consumption and generation in section III. In section IV a control architecture for the ST under the grid forming mode is proposed and simulation results are introduced. Section V demonstrates experimental results of a prototype before section V concludes the results of the work.

II. Smart Transformer Architecture

The conceptualization and design of the ST architecture is a challenging task, because of numerous choice options, such as topologies of power converter (for each power processing

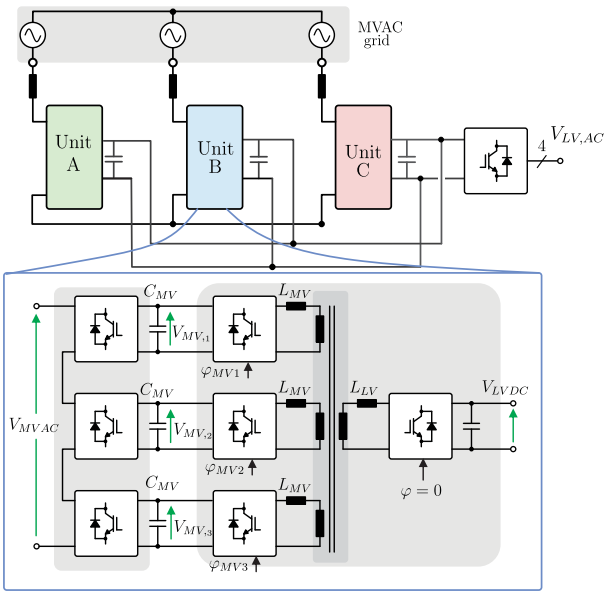

Fig. 2: ST architecture and circuit of the power unit used to implement the entire system.

stage), availability of dc links, number of modules and etc. In distribution grid application, the ST architecture is intended to have an advanced control system, in order to provide the required ancillary services to the grid. The architectures composed of the CHB (to implement the MV stage) and the multiple active bridges converter (to implement the DC-DC stage) offers the required degree of freedom to implement the control system, while providing high efficiency [12], [13]. Moreover, besides the advantage of power controlability and high efficiency [14], the QAB converter offers economical advantages over the DAB converter, as demonstrated in [15]. For these reason, the ST topology investigated in this work is based on the CHB and QAB converters, as depicted in Fig. 2. The system's specification and the parameters used in each converter are presented in Table I.

TABLE I: Technical specification of the ST demonstrator

System Specification	
System configuration	Three-phase
Total Power	90 kW
Input line-line voltage	2600 V_{rms}
Input line-neutral voltage	$V_{MVAC} = 1500\ V_{rms}$
Total MVDC link	$V_{MVDC} = 2400\ V$
Single MVDC link	$V_{MV} = 800\ V$
LVDC link	$V_{LV} = 800\ V$
CHB Parameters	
Nominal modulation index	$m = 0.8$
Switching frequency	$f_{s(CHB)} = 10\ kHz$
IGBT	IKW40N120T2 Infineon Technology $V_{block} = 1200\ V$ $V_{CE} = 1.75\ V$
Capacitor bank	$C_{MV} = 750\ \mu F$
QAB Parameters	
Transformer turn-ratio	$n = 1:1:1:1$
Switching frequency	$f_{s(QAB)} = 20\ kHz$
SiC-MOSFETs (LV side)	C2M0040120D Wolfspeed/CREE $V_{block} = 1200\ V$ $R_{DS(on)} = 40\ m\Omega$
SiC-MOSFETs (MV side)	C2M0025120D Wolfspeed/CREE $V_{block} = 1200\ V$ $R_{DS(on)} = 25\ m\Omega$

A. Power Converters

As observed in Fig. 2, an unit comprises a QAB converter associated with three CHB cells. One unit is used per phase, resulting then in three units for assembling the entire architecture. The circuit of the unit is also depicted in Fig. 2. To design the system and to define those components shown in Fig. 2, the specification presented in Table I and the equations provided in [16] have been used and the selected components are summarized in Table I.

As specified in Table I, the switching frequency of the CHB is 10 kHz, which leads to a effective frequency of 60 kHz on the filter. This frequency leads to low switching losses, while maintains low filter volume. In virtue of the low commutation frequency, IGBTs optimized for reducing the conduction losses can be properly employed and then the device IKW40N120T2 from *Infineon Technology* is adopted. This IGBT is recommended to application up to 10 kHz and it very suitable in this application.

The QAB converter, on the other hand, has a switching frequency of 20 kHz, which provides a good trade-off between magnetic elements volume and isolation issues due to the partial discharge, as discussed [17]. The SiC-MOSFETs from *Wolfspeed/CREE* were employed in both sides of the converter. The device C2M0040120D, which has a $R_{DS(on)} = 40\ m\Omega$ was used on the MV side, while the device C2M0025120D with $R_{DS(on)} = 25\ m\Omega$ was used on the LV side. The semiconductors with lower $R_{DS(on)}$ was selected for the LV side in order to reduce the conduction losses, once that the current level in this side is very high. The inductance and capacitance are also presented in Table I. To modulate the QAB converter, several strategies can be used, but the Phase-Shift Modulation (PSM) is the most used one. This scheme is characterized by zero voltage switching (ZVS) turn-on, but this features depends on the input and output voltages relation and also the load. As the input and output voltage are considered constant in ST application, the converter can be properly designed to work with ZVS operation for its entire range of operation. Thus, the modulation strategy is used in this work, where the phase of LV bridge is considered the reference to the others bridges. It means that $\varphi_{LV} = 0$, while the phase-shifts of the bridges connected in the MV side are defined as: φ_{MV1}, φ_{MV2} and φ_{MV3}, as illustrated in Fig. 2.

TABLE II: Parameters of Magnetic Cores

Parameter	Symbol	Core type	
		EE70/33/32	UU93/76/30
Magnetic path length	l_e	149 mm	354 mm
Cross section area	A_e	680 mm^2	840 mm^2
Mean turn length	l_w	65 mm	220 mm
Ferrite material type		TDK N87	
Effective permeability	μ_e	1700	1900
Saturation flux density	B_S	350 mT	

B. Design of Magnetic Components

Application of the QAB converter reduces drastically number of magnetic components, which results in their more complicated design. This subsection aims to elaborate on construction of magnetic components utilized in the given experimental prototype. Ferrite cores and Litz-wire windings are considered in this study due to use of switching frequency of 20 kHz in the QAB converter and effective switching frequency of 60 kHz in the CHB converter [18]. Also, off-the-shelf availability and minimization of core types are considered in design process. Two cores presented in Table II are preselected through iterative design procedure. Smaller ferrite core of EE70 type is selected for building QAB inductors placed in series with the transformer windings. The bigger ferrite core of UU93 type suits for realization of the isolation transformer and the grid-side inductor of the CHB converter. Due to high operating currents, design optimization is performed towards achieving minimum number of winding layers to minimize proximity power losses that cannot be suppressed only by means of the Litz-wire [18]–[20].

Inductors designed for the given experimental prototype need to store relatively high energy and, therefore, require relatively large air-gap to be introduced into a core. Parameters of the magnetic components designed are presented in Table III. Litz-wire from *Rupalit Safety* series with additional isolation is used to meet high isolation requirements. Evidently, large air-gap is used for the three inductor types designed, which require careful consideration of the magnetic flux fringing inside the air-gap. Flux fringing factor F characterizes this effect and could be calculated as follows [21]:

$$F = 1 + \frac{l_g}{\sqrt{k \cdot A_e}} \cdot \frac{2 \cdot l_w}{l_g}, \tag{1}$$

where l_g is the air-gap length, k is the number of the core sets, while the other parameters are defined in Table II. Maximum flux density B_{max} of the each inductor should be verified taking into account the flux frining factor F as follows [21]:

$$B_{max} = \frac{0.4 \cdot \pi \cdot N \cdot F \cdot I_{pk}}{l_g + \frac{l_e}{\mu_e}}, \tag{2}$$

where N is the number of turns, I_{pk} is the peak current that should be handled without saturation. As a results, maximum flux density is 302 mT (F=1.3), 308 mT (F=1.25) and 330 mT (F=1.6) for QAB LV port inductor, QAB MV port inductors and the CHB grid-side inductor, correspondingly. It is worth mentioning that the CHB grid-side inductor has two coils connected in parallel for higher current handling capability as shown in Fig. 3 (a). As a result, windings cover the both air-gap regions and measured fringing flux coefficient of 1.6 is below the value of 1.9 calculated using (1).

TABLE III: Parameters of Magnetic Components

QAB MV port inductor	
Inductance	75 μH
Core structure	2×EE70/33/32
Number of turns	9
Litz-wire	1260×0.071 mm
QAB LV port inductor	
Inductance	75 μH
Core structure	4×EE70/33/32
Number of turns	9
Litz-wire	512×0.1 mm (3 parallel)
CHB grid-side inductor	
Inductance	1 mH
Core structure	2×UU93/76/30
Number of turns	54
Litz-wire	512×0.1 mm (2 parallel)
Isolation transformer	
Number of windings	4
Turns ratio	1:1:1:1
Operating frequency	20 kHz
Number of turns	21
Litz-wire	508×0.1 mm

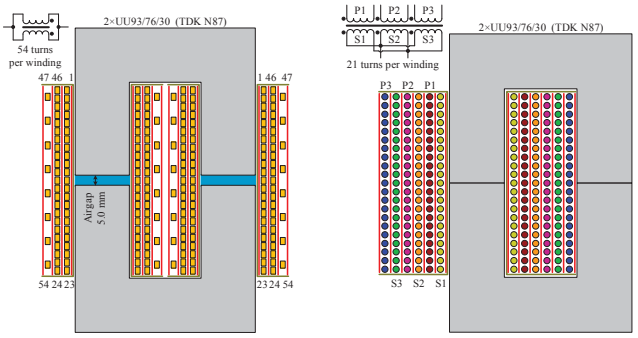

(a) (b)

Fig. 3: Sketch of (a) the CHB grid-side inductor and (b) the isolation transformer design.

Interleaved design of windings is used in the isolation transformer as shown in Fig. 3 (b). It allows achieving minimum leakage inductance and, consequently, enables one more degree of design freedom, when interchangeable external inductors are used to define power transfer characteristics of the given QAB converter [22]. However, interleaved windings results in increased concerns regarding isolation against the partial discharge that could be resolved with vacuum varnishing of the coil, reinforced isolation of the Litz-wire, etc. The minimal number of turns could be found as [23]:

$$N_{min} \geq \frac{V_{DC}}{4 \cdot B_S \cdot f_{SW} \cdot A_e \cdot k} = \frac{400 \cdot 10^3}{4 \cdot 0.35 \cdot 20 \cdot 840 \cdot 2} = 17, \tag{3}$$

where V_{DC} is the rated DC-link voltage, f_{SW} is the switching frequency of the QAB converter, and k is the number of the core sets. The transformer is designed with N = 21 turns, since this number fits into a single layer per winding and, consequently, results in low AC resistance of the windings and reasonable core flux density.

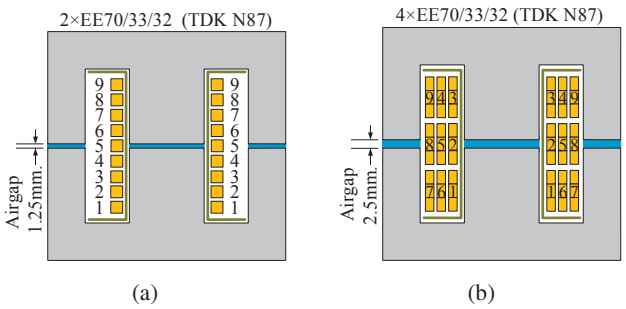

Fig. 4: Sketch of QAB (a) MV port and (b) LV port inductor design.

The QAB inductors have windings covering only one part of the air-gap and their inductance value predicted taking into account factor F corresponds to that measured. The QAB MV port inductor features 9 turns which are fitted into a single layer coil (Fig. 4 (a)) to minimize proximity effects. The design of the QAB LV port inductor results in 3-layer coil implementation due to use of three Litz-wires in parallel as shown in Fig. 4 (b).

III. Control of Smart Transformer allowing Universal Operation

This section describes the control variables for different operation modes of the ST based on Fig. 5, where the ST is displayed in connection to four grids. In the first scenario shown in Fig. 5 (a), the ST is acting like the traditional transformer: The ST is connected to a stiff MVAC grid and exchanges power to form a LVAC grid. The DC grids may absorb or inject power. Fig. 5 (b) instead shows the scenario, where no stiff AC grid is connected and the ST needs to form two AC grids. In the following, the different commands in the three stages are described along with potential solutions to influence the power consumption in the connected grids and therefore the power balancing capability of the ST, maximizing its time in operation and therefore the availability of the grid. A particular challenge for the operation of the system is the grid feeding mode on both AC grids connected to the ST as shown in Fig. 5 (b). This requires the active power to be fed by a DC grid or a storage system and is only feasible if the power is balanced. However, this may not be possible for all realistic operation modes and the power consumption and production in the AC grids is targeted to be affected. In order to do so, in the following subsections the control objectives are described along with the control variables to be manipulated in order to increase/decrease the power in the grid.

A. MV Stage

The MV stage of the ST is connecting the MVAC grid and the MVDC grid of the ST with the isolation stage. Traditionally, the MV grid is stiff and the MV stage operates in grid feeding operation as shown in Fig. 5 (a), enabling to absorb or to inject active power P_{MV} and reactive power Q_{MV}. In situations when there is a weak grid connected, the control of the active and the reactive power can be utilized to support the connected grid [5]. As an even more extreme case, the MVAC stage can operate in the grid forming mode and control the voltage of the grid $V_{MV,AC}$. This case is shown in Fig. 5 (b), where the AC grid voltage $V_{MV,AC}$ is controlled. In the grid feeding mode, the power in the AC grid can be manipulated by controlling the grid voltage $\Delta V_{MV,AC}$. In case of a constant impedance load, the active power is reduced for a reduction in the grid voltage. However, this does not apply for a constant power load [10]. Apart from the capability of controlling the power flow, in modular power converters, the power transferred by the individual building block can be controlled. The estimated potential to reduce or increase the voltage without violating the grid codes is expected to be $\Delta V_{MV,AC} = \pm 5\,\%$.

B. Isolation stage (QAB)

The control of the isolation stage aims at ensuring stable DC-links for the MV converters and the LV converters. Additionally, it needs to balance the MV converter cell voltages of a modular converter [24]. Depending if the converter in grid feeding operation is located in the MVDC side or in the LVDC side, either the LVDC link of the ST needs to be controlled or the accumulated MVDC link voltage. As a resulting challenge, the control objective needs to be changed if the grid feeding converter is changed from MV side to LV side or vice versa.

Apart from the power transfer between MV side and LV side, the isolation stage can be used to control the storage systems in a grid for balancing the power in the ST.

C. LV stage

The LV stage consists of a converter for the LVAC grid connection and a potential converter for the connection of a LVDC grid. Similar to the MV side, the converter can operate in the grid forming and the grid feeding mode with the similar control parameters voltage magnitude in the AC grid $\Delta V_{LV,AC}$ and fundamental frequency of the AC grid $\Delta f_{0,LV}$. Also in this case, it is expected to enable a voltage variation $\Delta V_{LV,AC} = \pm 5\,\%$ for reducing or increasing the power consumption in the grid [9].

IV. Configuration and Basic Control Strategy

A. Control strategy for the grid forming mode

This section proposes the control strategy for each stage under the grid forming mode as shown in Fig. 6. The control diagram for the MVAC side in the grid forming mode is shown in Fig. 6 (a), where the MVAC voltage (PI) and current (PR) controllers are structured in cascaded and the final references fed from the current controller are distributed to each cell in the CHB. A control algorithm for the QAB, which is shown in Fig. 6 (b), performs to balance the voltages of all DC-links, which affects a coupling of the MV side and the LV side. As a result, any of the connected AC or DC feeders or the storage system can control the active power in the system, implying that the control block is not required to change in according to the operation mode. Finally, Fig. 6 (c) presents the control block for the LV converter, which is always in the grid forming mode, and the control scheme is similar with that of the CHB under the grid forming mode.

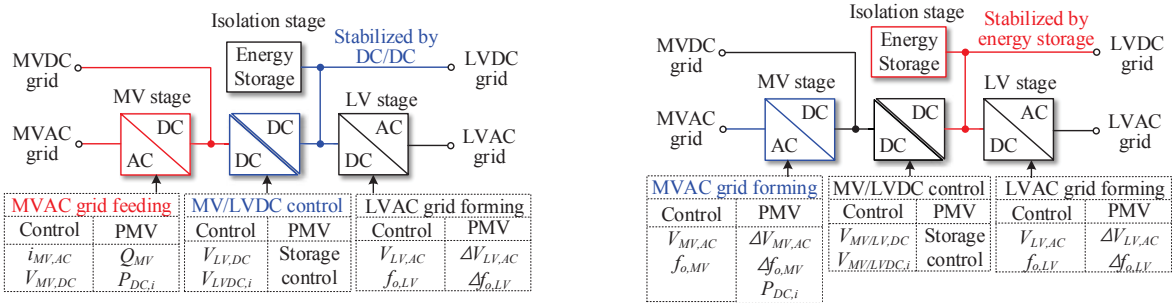

(a) (b)

Fig. 5: Potential operation scenarios with control and Power Manipulating Variables (PMV); (a) MV grid feeding and LV grid forming and (b) both MV and LV grid forming.

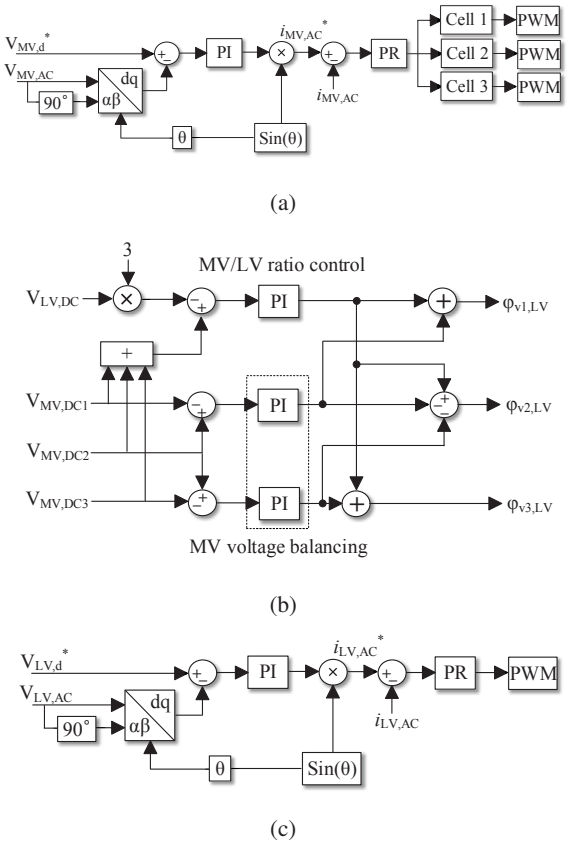

(a) (b) (c)

Fig. 6: Control block diagram for the grid forming mode: (a) CHB to control the MVAC, (b) QAB to control the MV/LVDC and (c) LV converter to control the LVAC.

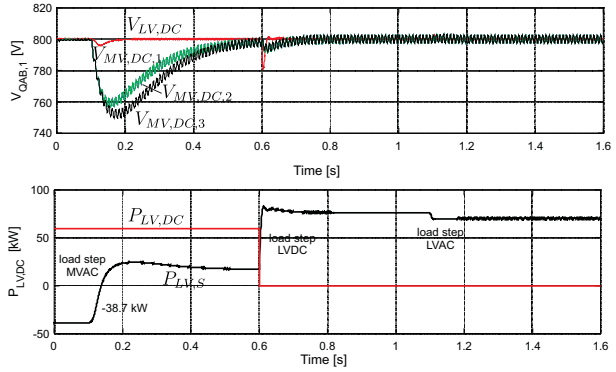

Fig. 7: Simulation of power steps and their influence on the voltage balancing of the QAB.

B. Simulation of the proposed control strategy

First the voltage balancing of the QAB is demonstrated in Fig. 7, which considers a ST architecture consisting of a QAB connected to a CHB in the MVAC side and a 2-level VSI on the LVAC side. The LVDC grid is injecting $P_{LV,DC} = 60\,kW$ and the storage system is balancing the active power by injecting or absorbing active power $P_{LV,S}$ in order to balance the power in the system. At $t = 0.1\,s$ load step in the MV grid occurs ($R_{MV} = 480\,\Omega \rightarrow R_{MV} = 87\,\Omega$) and at $t = 0.5\,s$ the power injection from the LVDC grid is stopped. The last occurrence is a load step in the LVAC grid from ($R_{LV} = 50\,\Omega \rightarrow R_{LV} = 11.5\,\Omega$). In order to show a robustness of the algorithm, the third leakage inductance of the MV side QAB is 20 % higher than the one of the others.

As it can be seen, the voltage balancing controller rejects all disturbances by means of power variations in the different grids. In addition, it can be seen that the voltage variations of the LVDC link and the MVDC links are coupled as it was targeted by the controller design.

The related MVAC and LVAC voltages and currents are shown in Fig. 8 (a), along with the power exchange with the storage system. In to reduce the power fluctuations and therefore increase the time for this potential operation mode as described in section III, it is proposed to control the grid voltage. This is shown in Fig. 8 (b). For minimizing the power transfer of the battery, the grid voltage is increased to 105 % of the nominal value in the LV side and the MV side for the time, when the energy system is absorbing power. The voltage is reduced to 95 % of its nominal value when the power transfer of the storage system reverses and therefore the power consumption in the AC grids is reduced. As it can be seen, the voltage increase affects a reduction of the power in the storage

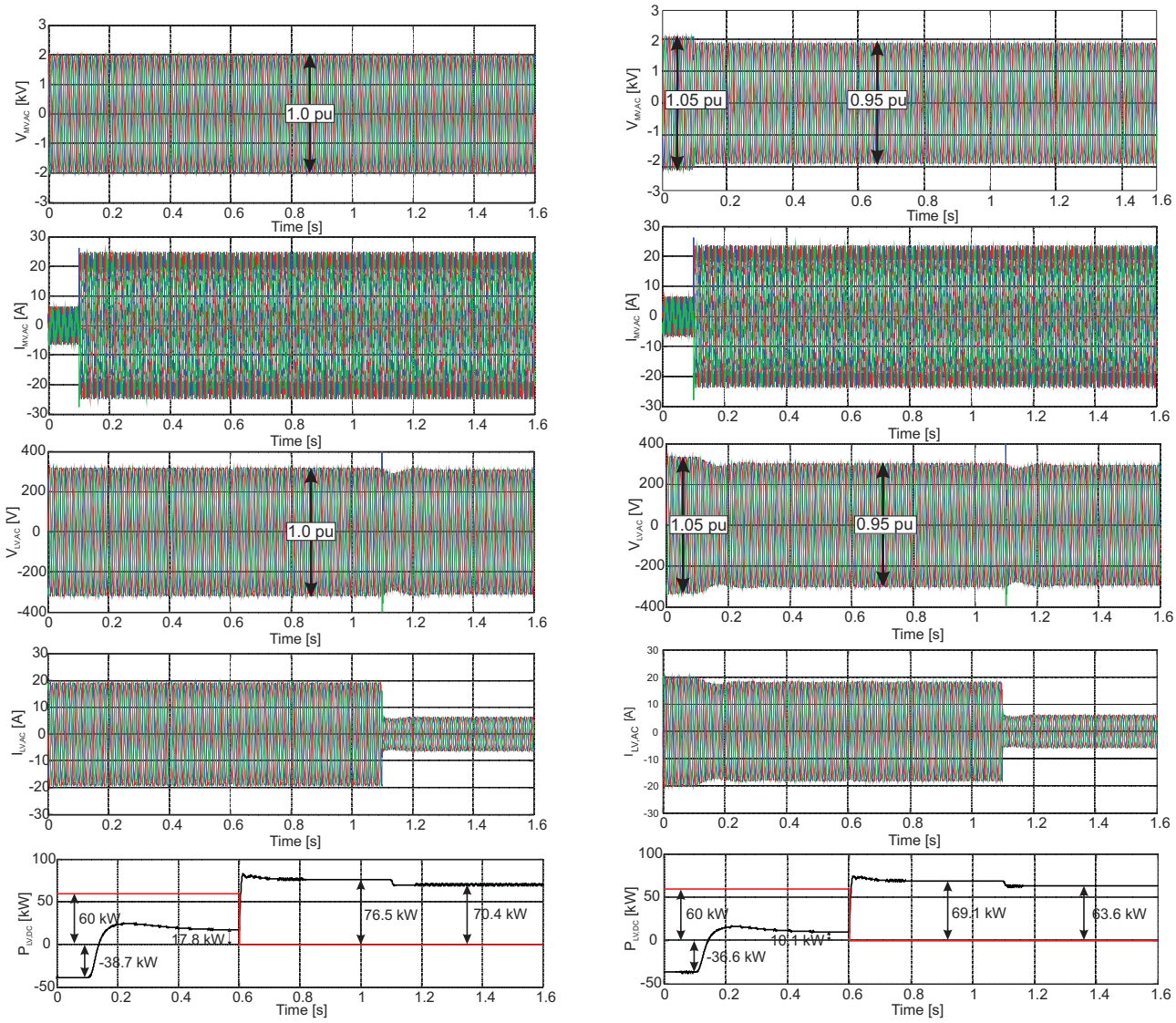

Fig. 8: Simulation of the power consumption of the LV and MV grid by means of grid voltage control: (a) for controlling the MV and LV grids to 100 % (b) by adapting the voltage reference in the MV and LV grids to 105 % (for $0s < t < 0.1s$) and 95 % (for $0.1s < t < 1.6s$).

system from $P_{LV,B} = -38.7kW \rightarrow P_{LV,B} = -36.6kW$ (by 5 %) before $t = 0.1s$ and even by 56 % at $t = 0.5s$. After $t = 0.6s$, when the grid is only consuming power, the reduction of the grid voltage affects a reduction of the power consumption by $\approx 10\%$. As a conclusion, the control of the grid voltage can effectively increase or reduce the power consumption in an AC grid, which is particularly powerful for grids with generation and consumption with a comparable power rating.

V. Experimental results

In this section, the developed prototype of semi-modular ST, which is shown in Fig. 9, is validated in terms of preliminary operating functionality. The prototype consists of single unit per phase, which involves 7-level CHB and QAB converters (see Fig. 2), and its specification is described in Table I. The CHB and QAB converters are controlled by individual *u*-Controller (MPC5643L), respectively. In more detail, each CHB/QAB converter is locally controlled by its own controller, which is called as slave controller, and the structure of the entire system is presented in terms of a communication network among the slave and master controllers in Fig. 10. The slave controllers for the CHB need to be synchronized in order to generate the three-phase voltage (i.e. 120° displacement) in addition to the central management for enabling and fault monitoring whereas those for the QAB converter perform solely for the central management. The Controller Area Network (CAN) 2.0B protocol is employed for this purpose.

Fig. 11 shows the availability for medium voltage operation with RL-load, where a DC source supplies 500 *V* to the LVDC and the total MVDC of 1500 *V* is regulated by QAB. As it is

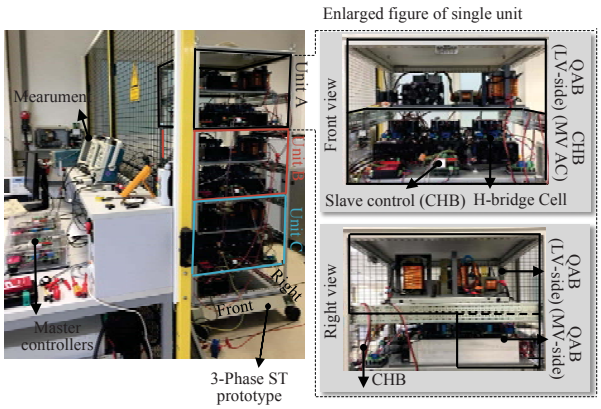

Fig. 9: Prototype of three-phase smart transformer consisting of single unit per phase.

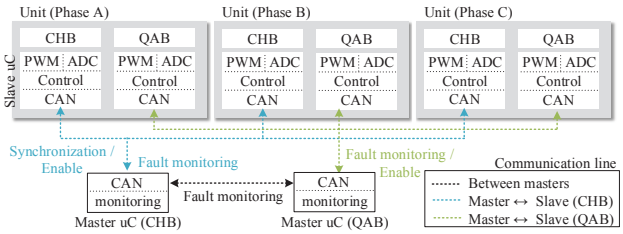

Fig. 10: Network structure among master/local controllers via CAN protocol.

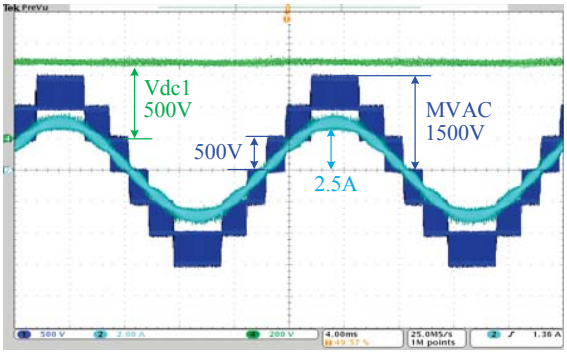

(a)

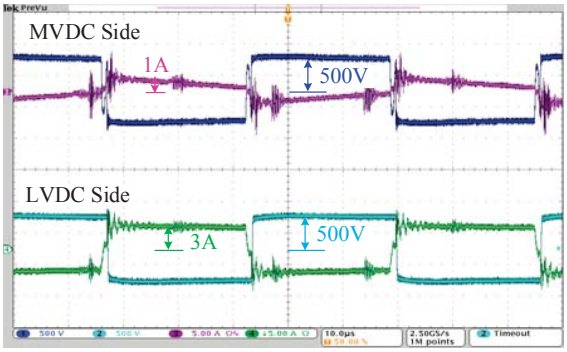

(b)

Fig. 11: Verification of medium voltage operation with a MVDC of 1.5 *kV* and RL-load; (a) CHB MVDC of one cell (green), MVAC (blue) and output current (light blue) and (b) QAB MVDC (upper) and LVDC (bottom) side voltage and current.

seen, the CHB output voltage before the filter evidently has the 7-level voltages, the output current is 2.5 A_{peak} and the MVDC of 500 *V* in one of cells is shown (Fig. 11 (a)). The QAB MVDC and LVDC side converter operation are simultaneously shown in Fig. 11 (b) with DC source of 500 *V* to the LVDC port.

As initial test phase, the prototype is operated under light load ($\geq$0.1 p.u.) due to a power limit of resistive load.

The control performance for the islanding mode, which was introduced in section III, is verified by step load change of $\pm$50 % as shown in Fig. 12, where the MVDC is 390 *V* and the MVAC is controlled to maintain 230 V_{rms}. The settling time is between 80 and 100 *ms* (12.5-10 *Hz*) and the fluctuation of around 0.1 p.u. is occurred in both cases.

Finally, the three-phase operation is demonstrated by synchronizing the slave controllers via the CAN network and the output voltages, which are exactly displaced by 120° with adjacent voltages, are achieved as shown in Fig. 13.

VI. Conclusion

The ST has been proposed as an interface between AC and DC grids with LV and MV rating. The design of a modular ST prototype consisting of a cascaded H-bridge converter and a quadruple active bridge converter has been presented along with the transformer design and the communication infrastructure for the system. A controller for the isolation stage is proposed, which achieves universal operation without changing the control variables in that stage. For manipulating the power injection into the connected grids, the AC grid voltages are proposed to be controlled in the grid forming operation. The capability is demonstrated to enable a reduction of $\approx$ 10 % in the active power for a reduction of the voltage by 5 %. Experimental results of the MV scale prototype were presented to demonstrate the grid forming operation of the system.

Acknowledgment

The research leading to these results has received funding from the European Union/Interreg V-A - Germany-Denmark, under the PE:Region Project and the European Research Council under the European Union's Seventh Framework Program (FP/2007-2013) / ERC Grant Agreement n. 616344 HEART, the Highly Efficient And reliable smart Transformer.

References

[1] A. Q. Huang, "Medium-voltage solid-state transformer: Technology for a smarter and resilient grid," *IEEE Industrial Electronics Magazine*, vol. 10, no. 3, pp. 29–42, Sept 2016.

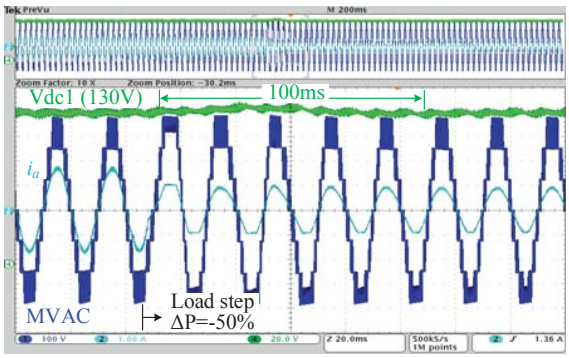

(a)

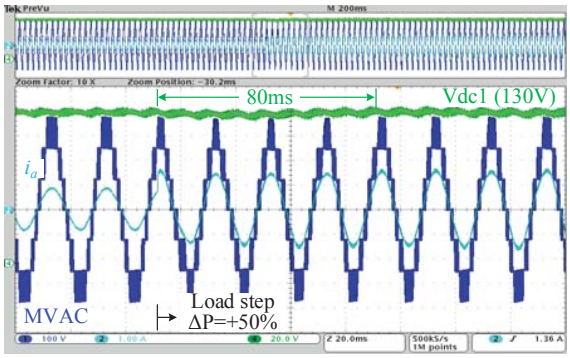

(b)

Fig. 12: Dynamic response of islanding mode control under step load change; (a) ΔP=-50% and (b) ΔP=+50%.

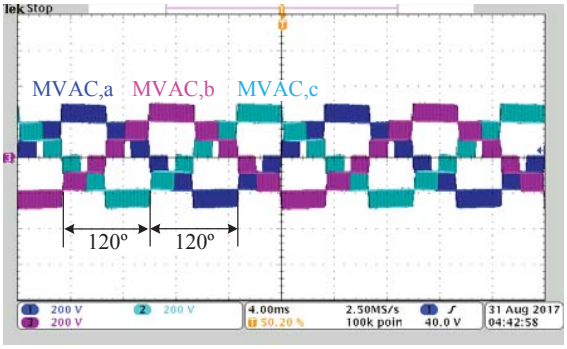

Fig. 13: Verification of synchronization among local controllers of CHB converter in each phase for three-phase operation.

[2] A. K. Sahoo and N. Mohan, "Modulation and control of a single-stage hvdc/ac solid state transformer using modular multilevel converter," in *2017 IEEE Applied Power Electronics Conference and Exposition (APEC)*, March 2017, pp. 1857–1864.

[3] M. Liserre, G. Buticchi, M. Andresen, G. D. Carne, L. F. Costa, and Z. X. Zou, "The smart transformer: Impact on the electric grid and technology challenges," *IEEE Industrial Electronics Magazine*, vol. 10, no. 2, pp. 46–58, June 2016.

[4] J. E. Huber and J. W. Kolar, "Solid-state transformers: On the origins and evolution of key concepts," *IEEE Industrial Electronics Magazine*, vol. 10, no. 3, pp. 19–28, Sept 2016.

[5] J. Rocabert, A. Luna, F. Blaabjerg, and P. Rodriguez, "Control of power converters in ac microgrids," *IEEE transactions on power electronics*, vol. 27, no. 11, pp. 4734–4749, 2012.

[6] C. Kumar, Z. Zou, and M. Liserre, "Smart transformer-based hybrid grid loads support in partial disconnection of mv/hv power system," in *2016 IEEE Energy Conversion Congress and Exposition (ECCE)*, Sept 2016, pp. 1–8.

[7] C. Kumar and M. Liserre, "A new prospective of smart transformer application: Dual microgrid (dmg) operation," in *IECON 2015 - 41st Annual Conference of the IEEE Industrial Electronics Society*, Nov 2015, pp. 004 482–004 487.

[8] ——, "Operation and control of smart transformer for improving performance of medium voltage power distribution system," in *2015 IEEE 6th International Symposium on Power Electronics for Distributed Generation Systems (PEDG)*, June 2015, pp. 1–6.

[9] G. Buticchi, D. Barater, M. Liserre, G. De Carne, and Z. Zou, *Analysis of the frequency-based control of a master/slave micro-grid*. IET, 2016.

[10] G. De Carne, G. Buticchi, M. Liserre, and C. Vournas, "Load control using sensitivity identification by means of smart transformer," *IEEE Transactions on Smart Grid*, 2016.

[11] Z.-X. Zou, G. De Carne, G. Buticchi, and M. Liserre, "Frequency adaptive control of a smart transformer-fed distribution grid," in *Applied Power Electronics Conference and Exposition (APEC), 2016 IEEE*. IEEE, 2016, pp. 3493–3499.

[12] J. E. Huber and J. W. Kolar, "Optimum number of cascaded cells for high-power medium-voltage ac-dc converters," *IEEE Journal of Emerging and Selected Topics in Power Electronics*, vol. 5, no. 1, pp. 213–232, March 2017.

[13] F. Krismer and J. W. Kolar, "Closed form solution for minimum conduction loss modulation of dab converters," *IEEE Transactions on Power Electronics*, vol. 27, no. 1, pp. 174–188, Jan 2012.

[14] L. F. Costa, G. D. Carne, G. Buticchi, and M. Liserre, "The smart transformer: A solid-state transformer tailored to provide ancillary services to the distribution grid," *IEEE Power Electronics Magazine*, vol. 4, no. 2, pp. 56–67, June 2017.

[15] L. F. Costa, F. Hoffmann, G. Buticchi, and M. Liserre, "Comparative analysis of mab dc-dc converters configurations in modular smart transformer," in *2017 IEEE 8th International Symposium on Power Electronics for Distributed Generation Systems (PEDG)*, April 2017, pp. 1–8.

[16] L. F. Costa, G. Buticchi, and M. Liserre, "Efficiency-cost trade-off design of a multiple-active-bridge converter for smart transformer," in *2018 IEEE Applied Power Electronics Conference and Exposition (APEC)*, March 2018.

[17] L. Costa, G. Buticchi, and M. Liserre, "Highly efficient and reliable sic-based dc-dc converter for smart transformer," *IEEE Transactions on Industrial Electronics*, vol. PP, no. 99, pp. 1–1, 2017.

[18] C. R. Sullivan, "Optimal choice for number of strands in a litz-wire transformer winding," *IEEE Transactions on Power Electronics*, vol. 14, no. 2, pp. 283–291, Mar 1999.

[19] C. R. Sullivan and L. W. Losses, "Analytical model for effects of twisting on litz-wire losses," in *2014 IEEE 15th Workshop on Control and Modeling for Power Electronics (COMPEL)*, June 2014, pp. 1–10.

[20] F. Tourkhani and P. Viarouge, "Accurate analytical model of winding losses in round litz wire windings," *IEEE Transactions on Magnetics*, vol. 37, no. 1, pp. 538–543, Jan 2001.

[21] C. W. T. McLyman, *Transformer and Inductor Design Handbook*. Marcel Dekker, 2004.

[22] A. Chub, L. Costa, and M. Liserre, "Analysis and design of asymmetric quad-active-bridge converter," in *Proc. IECON'2017*, 2017, pp. 5367–5372.

[23] M. K. Kazimierczuk, *High-Frequency Magnetic Components, 2nd Edition*. Wiley, 2013.

[24] S. Pugliese, M. Andresen, R. Mastromauro, G. Buticchi, S. Stasi, and M. Liserre, "Voltage balancing of modular smart transformers based on dual active bridges," in *2017 IEEE Energy Conversion Congress and Exposition (ECCE)*, Oct 2017, pp. 1270–1275.